Supplementary Materials for:

Electric Field-Induced Phosphorization to CoP@Biochar Composites for Efficient Bifunctional Oxygen Electrocatalysis

Xianli Wu,[a] Ting Zhou,[a] Teng Teng,[a] Shuling Liu,[a] Bangan Lu,[b] Sehrish Mehdia,[a] Yanyan Liu,[c,*] Jianchun Jiang,[d] Yongfeng Wang,[e] Baojun Li[a,f]

[a] College of Chemistry, Zhengzhou University,100 Science Road, Zhengzhou 450001, P. R. China

[b] College of Materials Science and Engineering, 100 Science Road, Zhengzhou 450001, P. R. China

[c] College of Science, Henan Agricultural University, 95 Wenhua Road, Zhengzhou 450002, P. R. China

E-mail: lyylhs180208@163.com (Y. Y. Liu)

[d] Institute of Chemistry Industry of Forest Products, CAF, National Engineering Lab for Biomass Chemical Utilization,16 Suojinwucun, Nanjing 210042, P. R. China

[e] Center for Carbon-based Electronics and Key Laboratory for the Physics and Chemistry of Nanodevices, School of Electronics, Peking University, Beijing 100871, P. R. China

[f] Department of Chemistry, Tsinghua University, Beijing 100084, P. R. China

Total number of pages: 18

Total number of figures: 22

Total number of tables: 4

Table of Contents

I. Materials and Methods

1.1 Electrochemical measurements:

All electrochemical measurements of ORR were performed on a CHI 760E Electrochemical Analyzer with rotating disk electrode (RDE) or rotating ring disk electrode (RRDE) as working electrode, Pt wire as the counter electrode, and Ag/AgCl as reference electrode. The working electrodes were bought from Pine. The electrolyte of reference electrode is saturated KCl solution. All potential values were converted to potential versus reversible hydrogen electrode (RHE) according to the following calculation:

$$E_{vs.RHE} = E_{vs.Ag/AgCl} + 0.059pH + 0.197 \qquad (1)$$

The electrode working area of the rotating disk electrode (RDE) is 0.196 cm^{-2} and the rotating ring-disk electrode (RRDE) is 0.217 cm^{-2}. The RRDE consists of a glassy carbon disk (GC) surrounded by a Pt ring, while there is only a GC in the center of the RDE. The catalyst ink was prepared by ultrasonic dispersion of 4 mg catalyst in a hybrid solution including 500 μL ethanol and 50 μL Nafion. 15 μL ink was coated onto working electrode. Before the electrochemical test, the glass reaction vessel and the vent should be boiled with deionized water. After drying, the glass cell was immersed in strong alkaline solution to remove any possible metallic impurities. Cyclic voltammetry (CV) measurements were carried out in O_2/N_2-saturated 0.1 M KOH solution in the voltage range of 0 - 1.2 V for all the samples with a scan rate of 50 mV s^{-1}. LSV test was performed in O_2- saturated 0.1 m KOH solution at different rotating speeds. The test range was 0.2 - 1.2 V (vs RHE) and the scan rate was 5 mV s^{-1}. The velocity of airflow was adjusted to 40 sccm. The accelerated durability test (ADT) was performed by CV in 0.1 M O_2-saturated KOH solution for 5000 cycles with a scan rate of 50 mV s^{-1}. Methanol resistance was measured by adding methanol to 100 mL 0.1 M KOH under 800 rpm at the 400th second. The concentration of CH_3OH in the electrolyte was 1 M. The i–t test was performed at 0.8 V for 22 h in O_2-saturated 0.1 M KOH solution at 800 rpm.

Tafel slopes were obtained from the Tafel equation:

$$E = \mathrm{a} + b\log|J_k| \qquad (2)$$

E is the applied potential of LSV tests, a is a constant, b is the Tafel slope and J_k is the kinetic current density.

Moreover, Kinetic properties of ORR were also carried out with RRDE in an O_2-saturated 0.1 M KOH solution with a scan rate of 5 mV s^{-1}. The yields of peroxide species and the electron transfer number can be calculated from the LSV of RRDE measurement at 1600 rpm via as following equation:

$$[H_2O_2]\% = 200 \times \frac{I_R/N}{I_R/N + I_D} \qquad (3)$$

$$\mathrm{n} = 4 \times \frac{I_D}{I_D + I_R/N} \qquad (4)$$

The I_D is the disk current and I_R is the ring current, respectively. The N represents the current collection efficiency equaled to 0.41 of the RRDE in our experimental system.

The LSV test for OER was also performed in N_2-saturated KOH solution. A Pt wire was used as the counter electrode and an Ag/AgCl electrode was used as the reference. The working electrode was fabricated via a similar method to ORR test. The measurement was performed in 1.1 - 1.9 V (vs RHE) with the scan rate of 5 mV s^{-1}. The OER stability was determined by i–t responses at 800 rpm at the potential of 1.56 V.

1.2 Assembly method of zinc-air battery

Liquid zinc-air battery: The home-made liquid ZAB was constructed in a custom mold. CoP@NWC ink was uniformly dispersed onto the hydrophobic carbon paper and dried at 60°C for 2h to get the cathode. The catalyst loading was 1.0 mg cm^{-2}. A piece of zinc plate was used as the anode, and 6 M KOH+0.2 M $Zn(Ac)_2$ aqueous solution was the electrolyte. The galvanostatic charge and discharge test was conducted using an automatic battery testing system (Neware CT-3008) with 20 min for each cycle (discharge, 10 min. charge, 10 min) at 10 mA cm^{-2}. Polarization data (v–i) were collected using LSV at a scan rate of 10 mV s^{-1}. The current and power density curves were calculated from the LSV curves. All tests were

performed in a natural environment at room temperature. The energy density of zinc-air battery was calculated based on the applied current (I), service hours (t), and the weight of consumed zinc (m_{Zn}).

$$Specific\ capacity\ (mA\ h\ g^{-1}) = (I \times t)/m_{Zn} \qquad (5)$$

Quasi-solid-state zinc-air battery: The quasi-solid-state ZABs were fabricated with a polished Zn foil as anode, CoP@NWC as freestanding air cathode and polyvinyl alcohol (PVA) as electrolyte. The PVA powder gel electrolyte was prepared via heating, freezing, and thawing procedure. The test method and conditions are same as that of liquid ZAB.

1.3 The detail of DFT calculations

All Spin-polarization density functional theory (DFT) calculations were performed by the first-principles. The electron exchange and correlation energy were treated within the generalized gradient approximation in the Perdew-Burke-Ernzerhof function (GGA-PBE). We have chosen the projected augmented wave (PAW) potentials to describe the ionic cores and take valence electrons into account using a plane wave basis set with a kinetic energy cutoff of 520 eV. The electronic energy was considered self-consistent when the energy change was smaller than 10^{-6} eV. A geometry optimization was considered convergent when the energy change was smaller than 0.03 eV $Å^{-1}$. In our structure, the U correction is used for Co atoms (5.83 eV). The vacuum spacing in a direction perpendicular to the plane of the structure is 20 Å for the surfaces. The Brillouin zone integration is performed using 3×3×1 Monkhorst-Pack k-point sampling for a structure. Finally, the adsorption energies (E_{ads}) were calculated as $E_{ads}= E_{ad/sub} -E_{ad} -E_{sub}$, where $E_{ad/sub}$, E_{ad}, and E_{sub} are the total energies of the optimized adsorbate/substrate system, the adsorbate in the structure, and the clean substrate, respectively. The free energy was calculated using the equation:

$$G = E_{\mathrm{ads}} + ZPE - TS \qquad (6)$$

where G, E_{ads}, ZPE and TS are the free energy, total energy from DFT calculations, zero point energy and entropic contributions, respectively.

II. Supplementary Figures and Tables

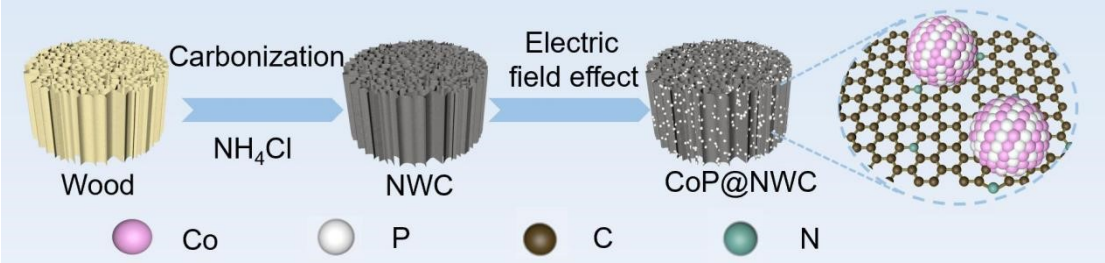

Figure S1. Illustration for the construction of CoP@NWC.

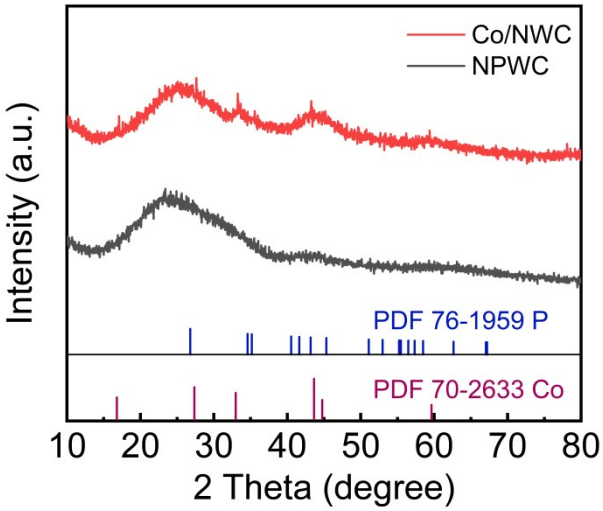

Figure S2. XRD patterns of Co/NWC and NPWC.

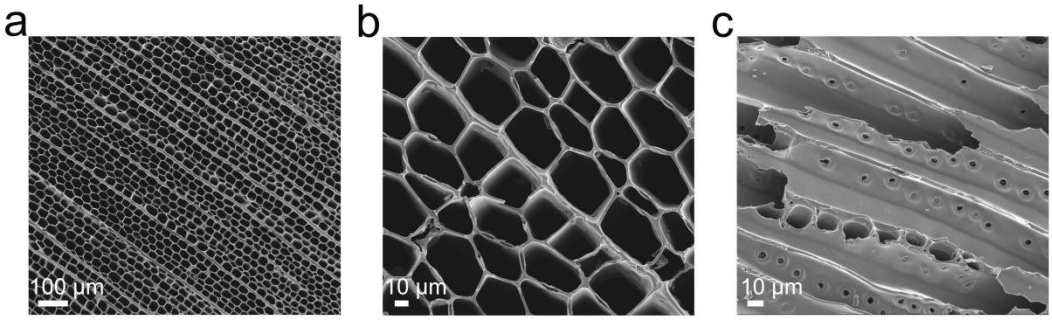

Figure S3. SEM images of WC, (a, b) SEM of WC (parallel). (c) SEM of WC (vertical).

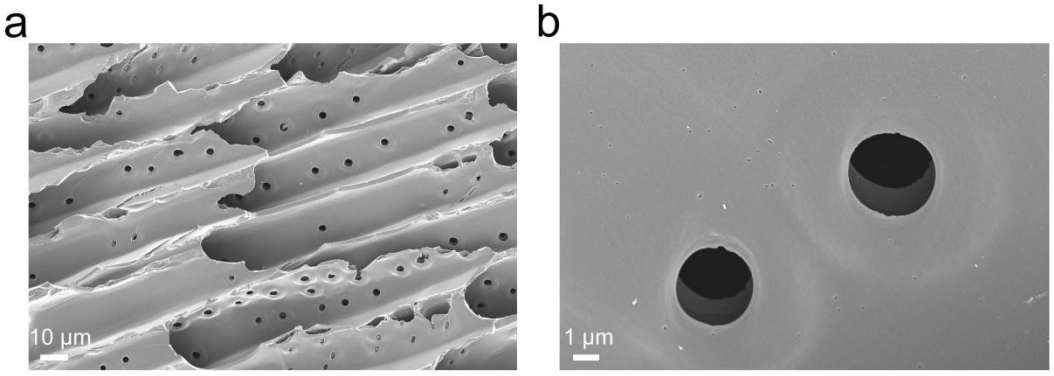

Figure S4. SEM images of NWC, (a, b) SEM images of NWC. (vertical).

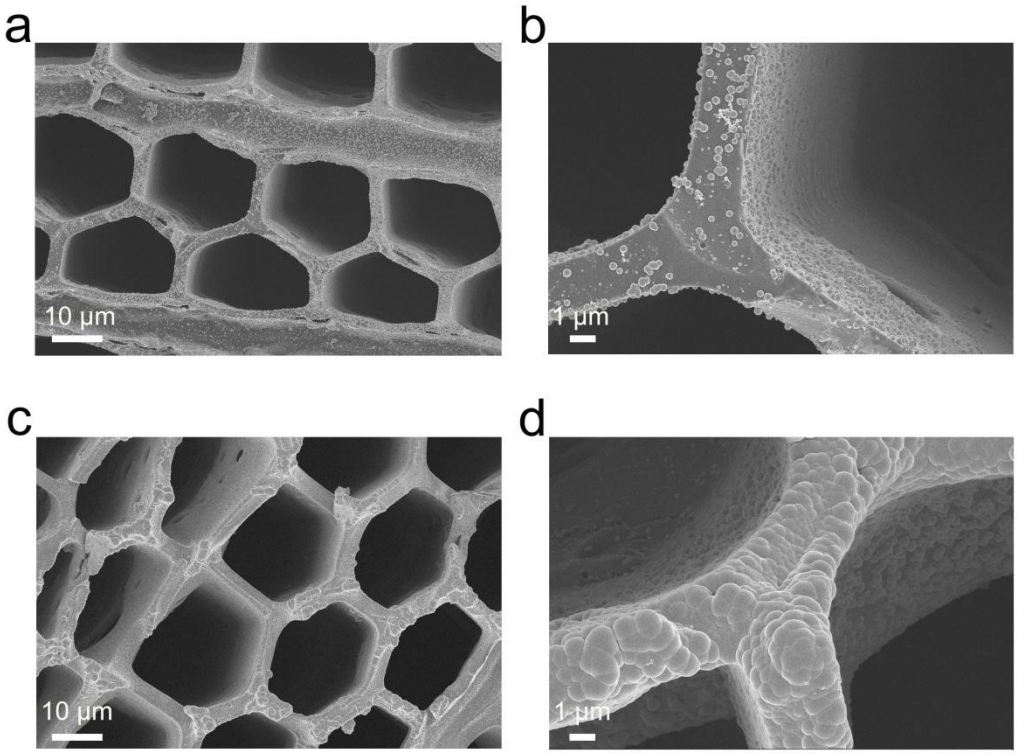

Figure S5. (a, b) SEM images of CoP@NWC-1, (c, d) SEM images of CoP@NWC-2.

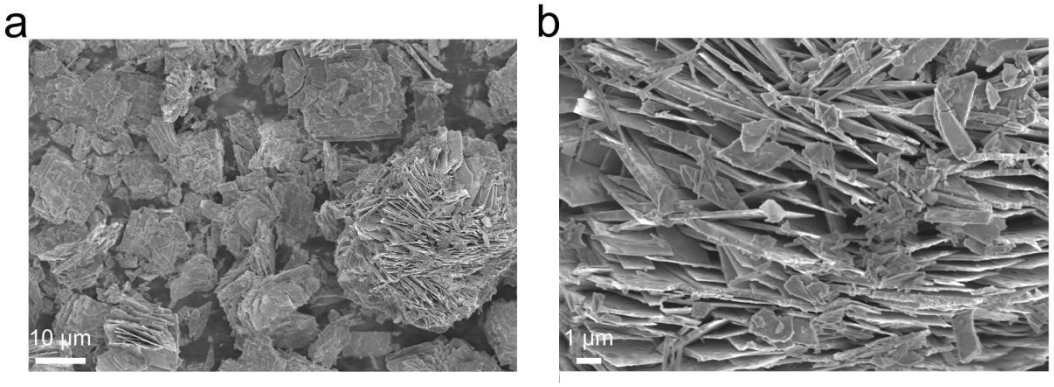

Figure S6. SEM images of pure CoP.

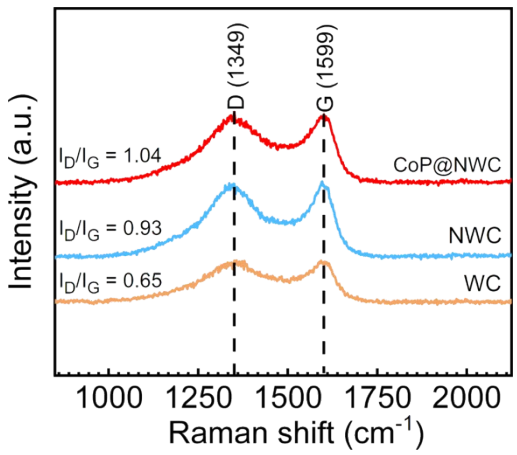

Figure S7. Raman spectra of WC, NWC and CoP@NWC.

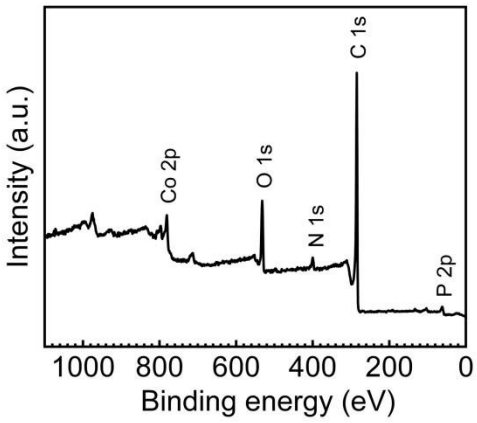

Figure S8. X-ray photoelectron spectroscopy (XPS) survey spectrum of CoP@NWC.

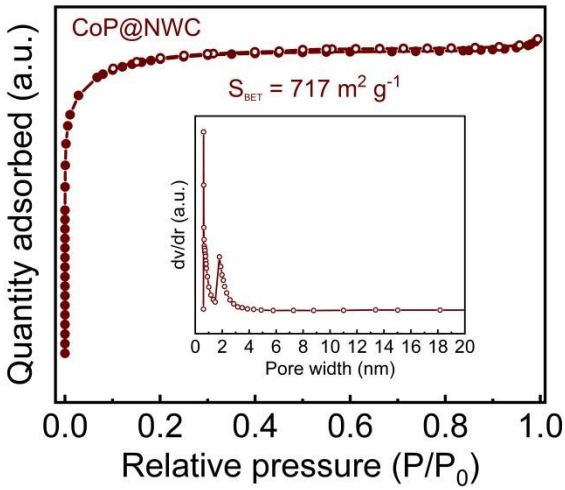

Figure S9. N_2 adsorption-desorption isotherms of CoP@NWC.

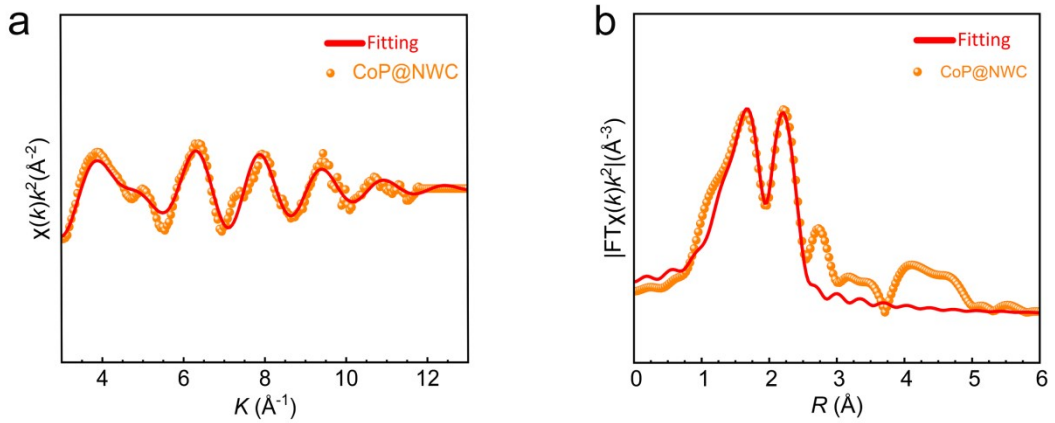

Figure S10. (a) EXAFS fitting result of CoP@NWC catalyst in *k* space. (b) The corresponding fitting curve of Fourier-transformed EXAFS spectra of CoP@NWC catalyst in *R* space.

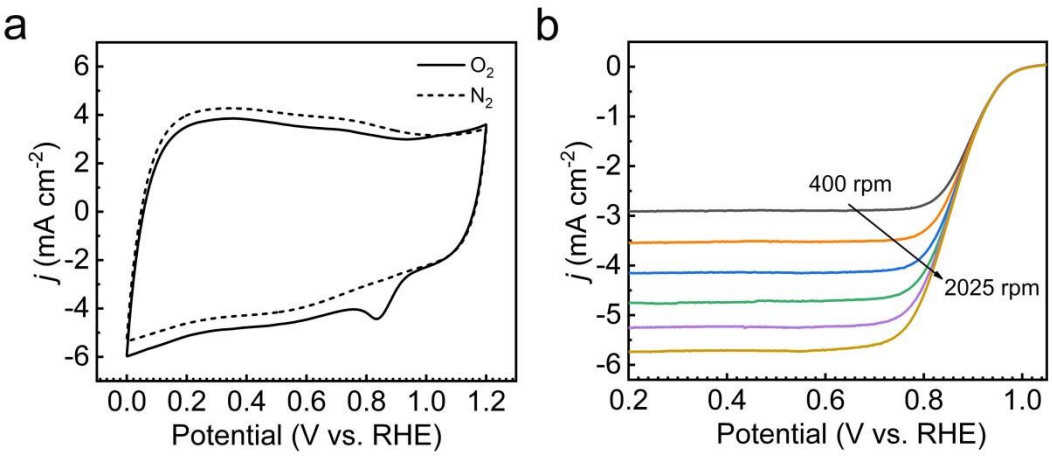

Figure S11. (a) CV curves of CoP@NWC, (b) LSV curve of CoP@NWC at different rotation speed.

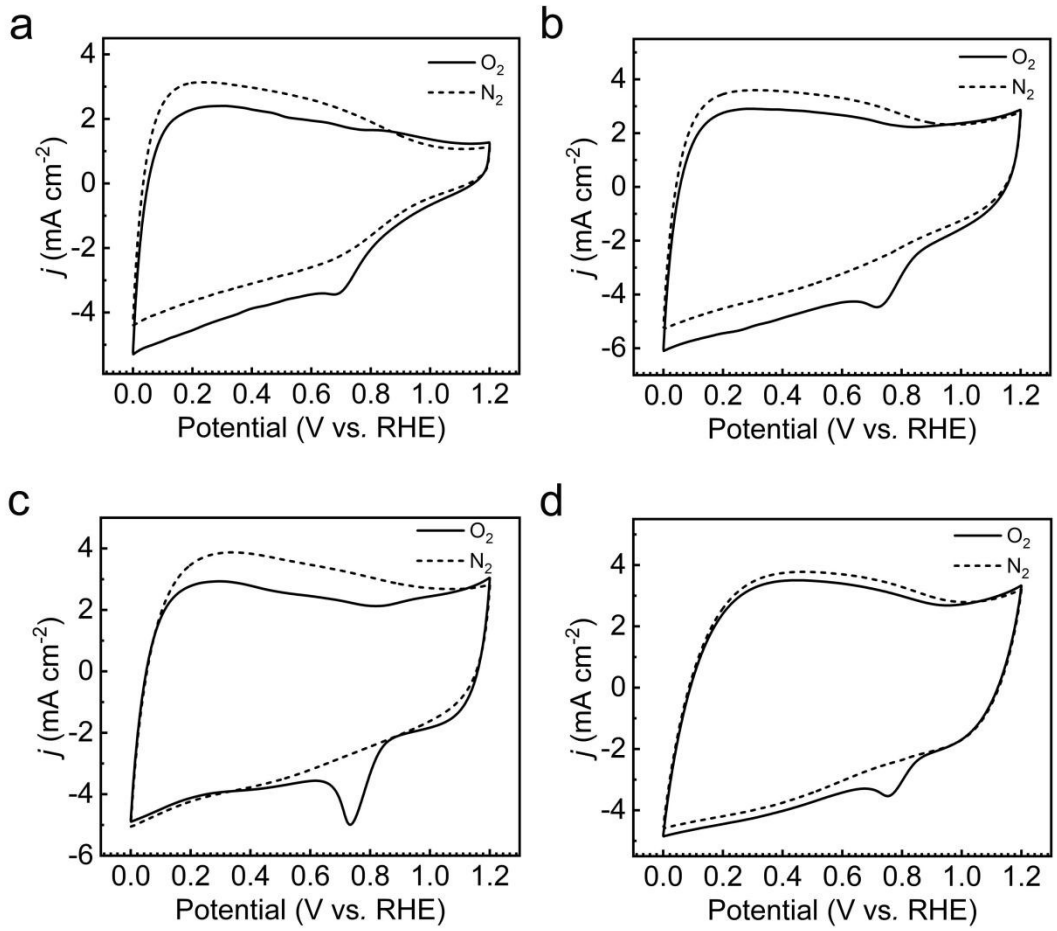

Figure S12. CV curve of (a) WC, (b) CoP, (c) CoP@WC, (d)NWC.

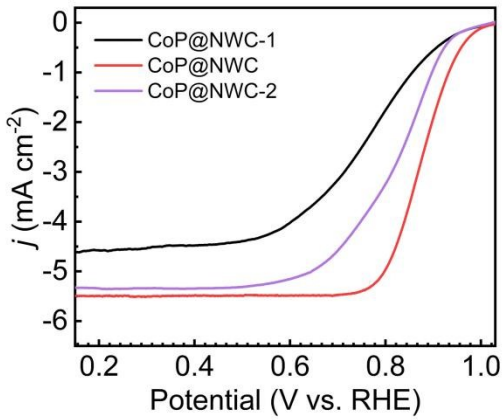

Figure S13. LSV curves of CoP@NWC, CoP@NWC-1 and CoP@NWC-2 for the ORR with a rotating rate of 1600 rpm in O_2-saturated 0.1 M KOH.

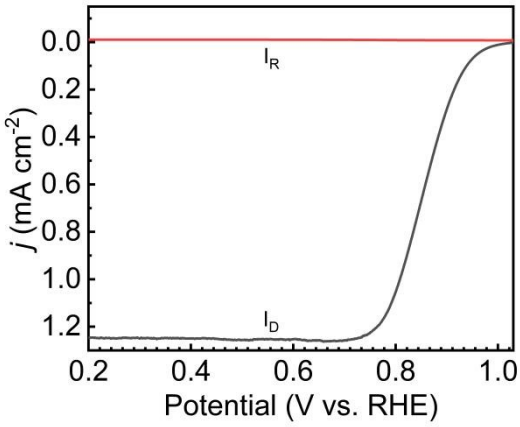

Figure S14. Disk and ring currents obtained by LSV on a RRDE for CoP@NWC.

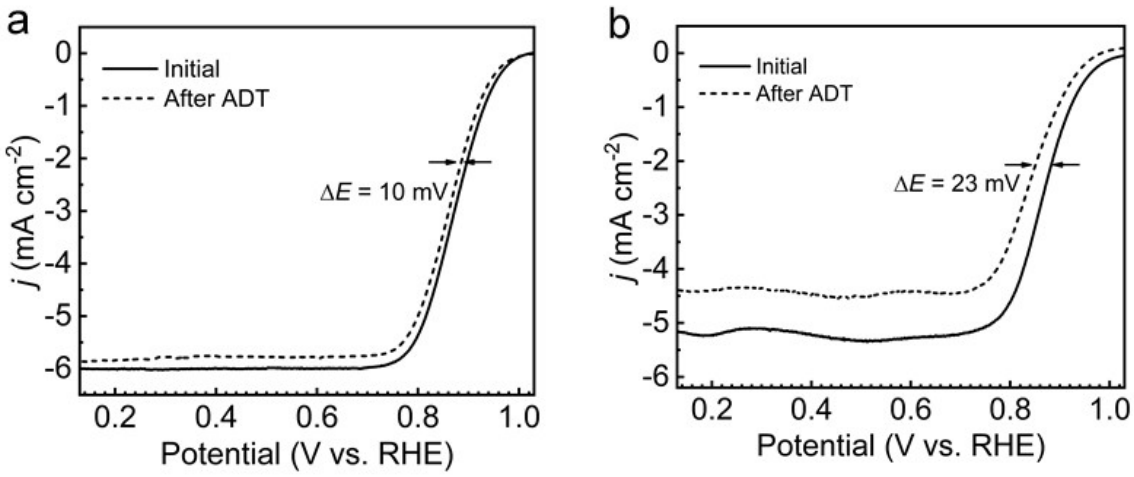

Figure S15. LSV curves before and after 5000 cycles of (a) CoP@NWC and (b) Pt/C.

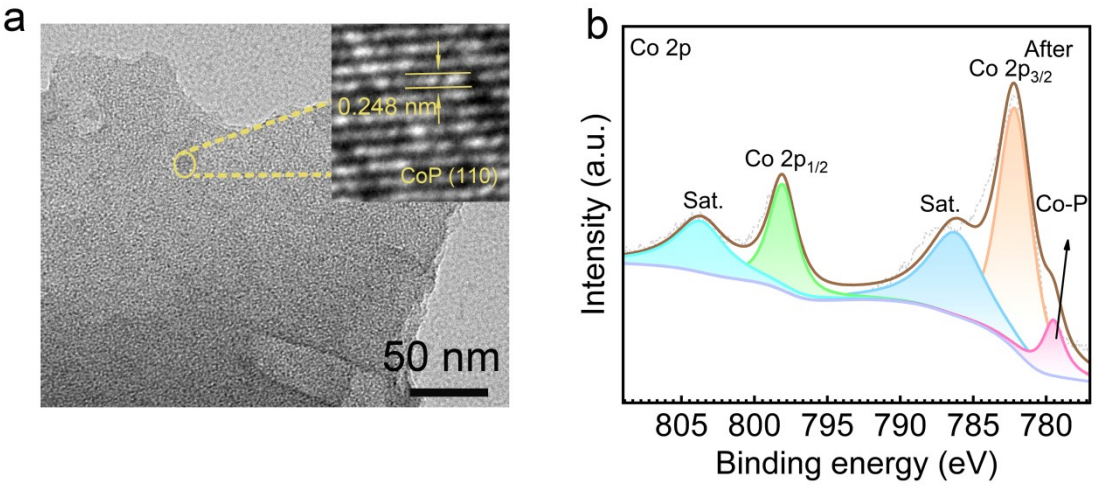

Figure S16. (a) TEM images, (b) High-resolution XPS spectrum of Co 2p of CoP@NWC after reaction.

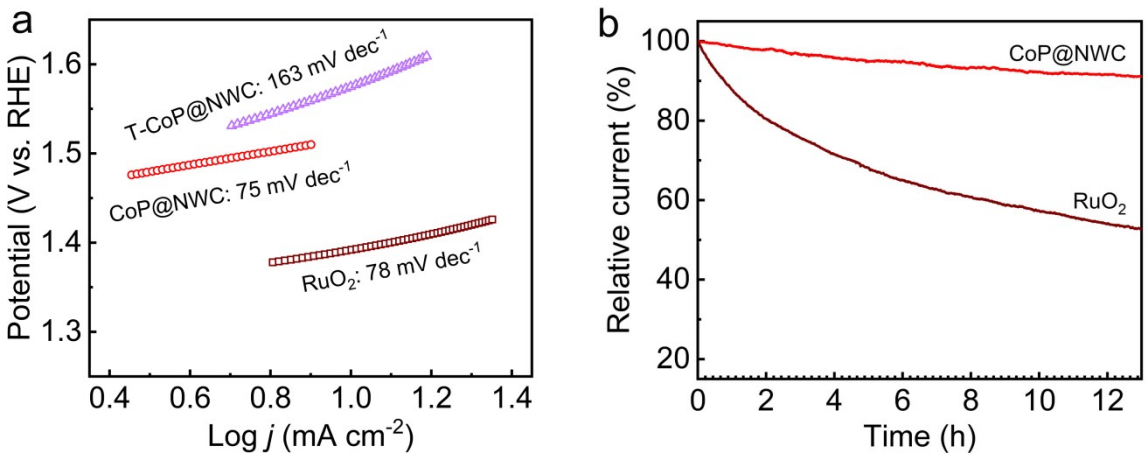

Figure S17. (a) Tafel plots for OER on different catalysts. (b) chronoamperometry (CP) response on CoP@NWC and RuO_2.

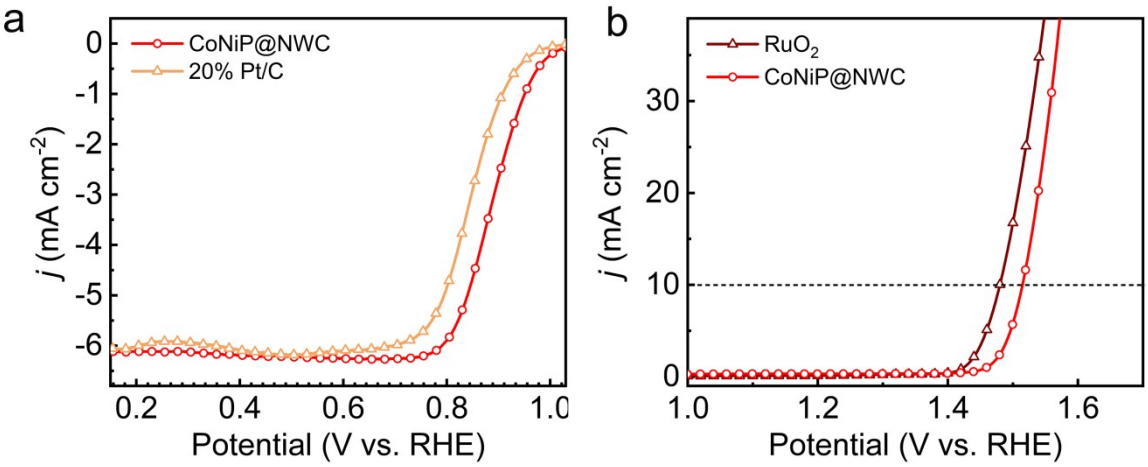

Figure S18. (a) LSV curves of CoNiP@NWC and 20% Pt/C. (b) OER LSV curves of CoNiP@NWC and RuO_2.

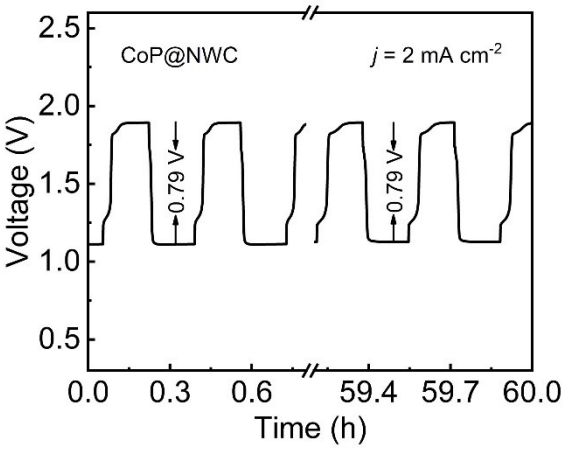

Figure S19. The voltage gap of solid-state ZAB based on CoP@NWC.

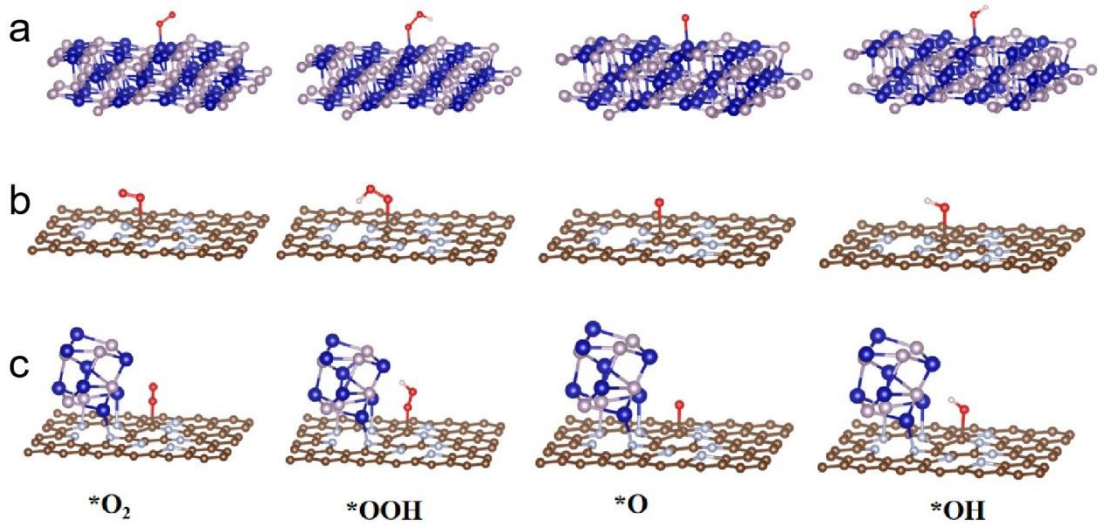

Figure S20. The configurations for adsorbates (*O_2, *OOH, *O, *OH) on (a) CoP, (b) CoP@NWC and (c) NWC**.** The blue, purple, brown, white, red, and pink balls represent Co, P, C, N, O, and H atoms, respectively.

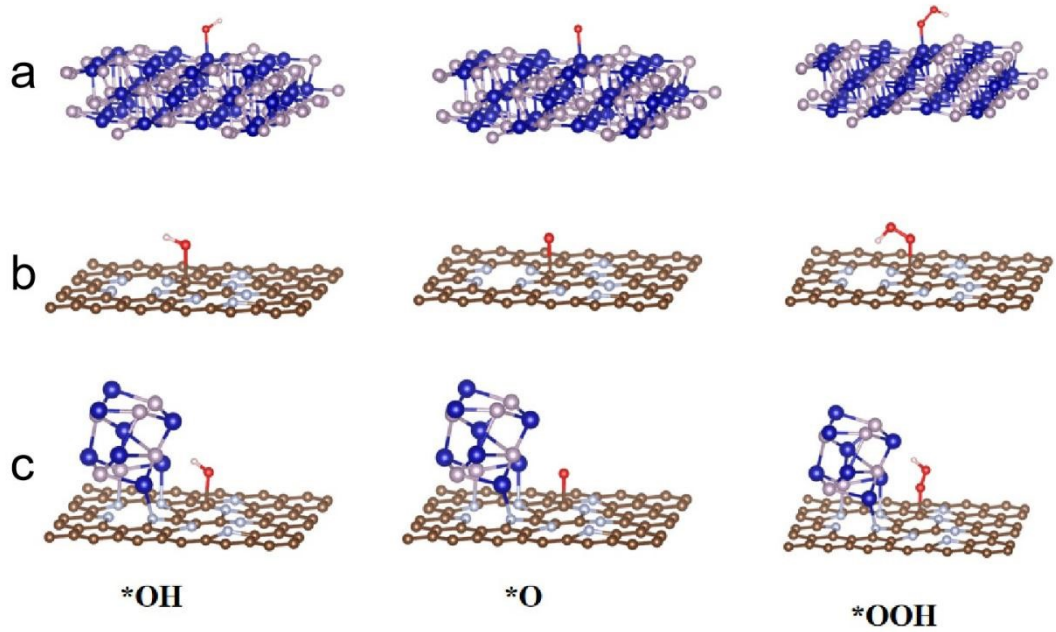

Figure S21. The configurations for adsorbates (*OH, *O, *OOH) on (a) CoP, (b) CoP@NWC and (c) NWC**.** The blue, purple, brown, white, red, and pink balls represent Co, P, C, N, O, and H atoms, respectively.

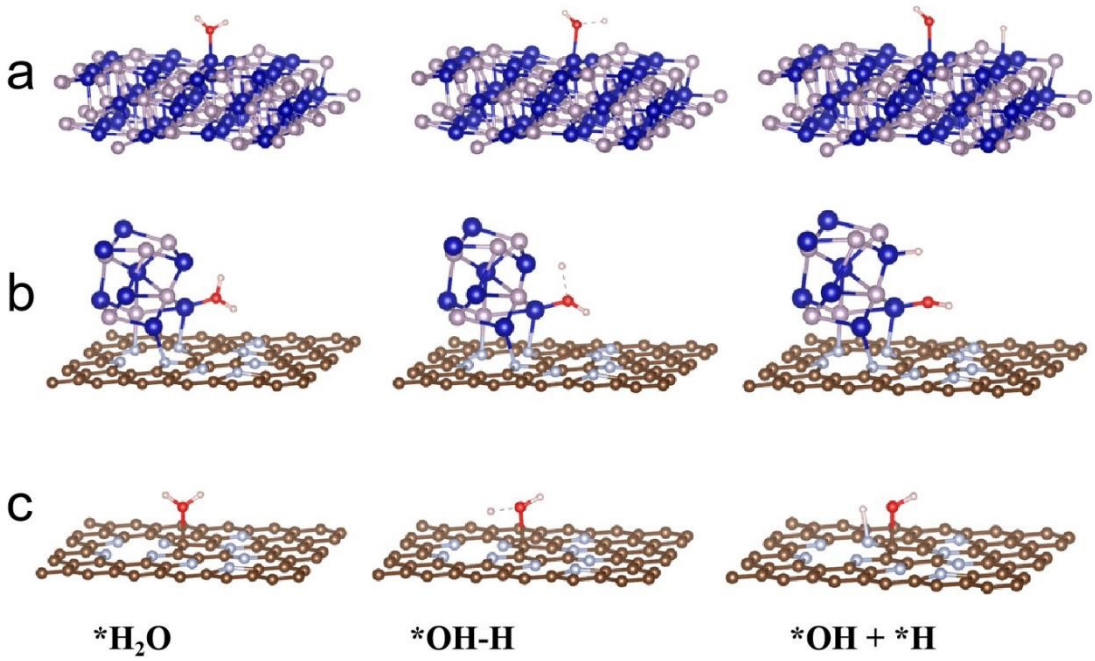

Figure S22. The configurations of the adsorption and dissociation of H_2O on (a) CoP, (b) CoP@NWC and (c) NWC. The blue, purple, brown, white, red, and pink balls represent Co, P, C, N, O, and H atoms, respectively.

Table S1. EXAFS fitting parameters at the Co K-edge for Co foil, CoO, Co_3O_4, CoP, CoP@NWC.

Sample	Shell	*CN*[a]	*R*(Å)[b]	σ^2(Å^2)[c]	ΔE_0(eV)[d]	*R* factor
Co foil	Co-Co	12*	2.49	0.0061	7.03	0.0015
CoO	Co-O	6*	2.12	0.0067	0.39	0.0041
	Co-Co	18*	3.01	0.0099	-2.74	
Co_3O_4	Co-O	4*	1.92	0.0013	-4.84	0.0055
	Co-Co1	6*	2.87	0.0058	-6.60	
	Co-Co2	6*	3.76	0.0043	-6.60	
CoP	Co-P	2.4	2.22	0.0066	-6.52	0.0033
	Co-Co	14.4	2.49	0.0221	-13.89	
CoP@NWC	Co-P	6.1	2.30	0.0109	-8.06	0.0063
	Co-Co	5.9	2.45	0.0142	-1.99	

Table S2. Comparison of electrocatalytic OER and ORR activity

Catalysts	$E_{ORRonset}$ [V]	$E_{ORR1/2}$ [V]	E_{OER}[V] (j=10 mA·cm^{-2})	△E[V] ($E_{j=10}$–$E_{1/2}$)	Ref.
CoP@NWC	**0.99**	**0.87**	**1.52**	**0.65**	**This Work**
CoP-PBSCF	-	0.752	1.61	0.858	[1]
CoP@PNC-DoS	0.94	0.803	1.584	0.781	[2]
Co_xP@NPC	-	0.82	1.57	0.75	[3]
CoP-DC	-	0.81	1.55	0.74	[4]
Co/CoP-HNC	0.94	0.83	1.62	0.79	[5]
$Co(OH)_2$@NC	-	0.83	1.52	0.69	[6]
Co/Co_2P@NCNTs	-	0.90	1.58	0.68	[7]
Co/SiO_x/NC	-	0.81	1.493	0.68	[8]
CoFe/SN-C	-	0.855	1.588	0.73	[9]
Co@N-CNT	-	0.84	1.72	0.87	[10]
CoFe@NC/KB	-	0.845	1.615	0.77	[11]

Table S3. Liquid ZABs performances of some previous literature of nonprecious metal.

Catalysts	Open circuit potential (V)	Power density (mW cm^{-2})	Specific capacity ($mAh \cdot g_{Zn}^{-1}$)	Durability	Ref.
CoP@NWC	**1.50**	**175**	**805.8**	**407h@10 mA cm^{-2}**	**This Work**
CoP-N/P-C-850	1.46	151	773.8	85h@5mA cm^{-2}	[12]
CoFe/N-HCSs	1.38	96.5	777.4	160h@5mA cm^{-2}	[13]
Co_2P/CoNPC	1.425	116	-	60h@10mA cm^{-2}	[14]
N-CoS_2 YSSs	1.41	81	744	165h@10 mA cm^{-2}	[15]
Co_3HITP_2	1.47	164	784	80h@5mA cm^{-2}	[16]
(Zn,Co)/NSC	1.5	150	-	22h@5mA cm^{-2}	[17]
$NiCo_2O_4$/MXene	1.4	-	768.6	333h@5mA cm^{-2}	[18]
NiFe@N-CFs	1.4	102	696	40min@10 mA cm^{-2}	[19]

Table S4. All-solid-state ZABs performances of previous literature of nonprecious metal.

Catalysts	Open circuit potential (V)	Power density (mW cm^{-2})	Durability	Ref.
CoP@NWC	**1.44**	**76**	**60h@2 mA cm^{-2}**	**This Work**
CoFe/N-HCSs	1.40	-	10h@1 mA cm^{-2}	[13]
Co-SAs@NC	1.40		12h@2 mA cm^{-2}	[20]
CoP_x /Co-N_x-C@CNT	1.36	59	1400min@5 mA cm^{-2}	[21]
NPC/FeCo@NCNT	1.45	65	400min@1 mA cm^{-2}	[22]
$NiCo_2O_4$@NiCoFe-OH	1.36	31.8	15h@2 mA cm^{-2}	[23]
Co-NCF	-	25	10h@2 mA cm^{-2}	[24]
Co@NCNTA-700	-	38.6	18h@1 mA cm^{-2}	[25]

Reference

1. Y.-Q. Zhang, H.-B. Tao, Z. Chen, M. Li, Y.-F. Sun, B. Hua, J.-L. Luo, *J. Mater. Chem. A* 2019, **7**, 26607.

2. Y. Li, Y. Liu, Q. Qian, G. Wang, G. Zhang, *Energy Storage Mater.* 2020, **28**, 27.

3. Q. Shi, Q. Liu, Y. Zheng, Y. Dong, L. Wang, H. Liu, W. Yang, *Energy Environ. Mater.* 2022, **5,** 515.

4. Y. Lin, L. Yang, Y. Zhang, H. Jiang, Z. Xiao, C. Wu, G. Zhang, J. Jiang, L. Song, *Adv. Energy Mater.* 2018, **8**, 1703623.

5. Y. Hao, Y. Xu, W. Liu, X. Sun, *Mater. Horiz.* 2018, **5**, 108.

6. Y. Wang, A. Li, C. Cheng, *Small* 2021, **17**, 2101720.

7. M. Wu, G. Zhang, N. Chen, Y. Hu, T. Regier, D. Rawach, S. Sun, *ACS Energy Lett.* 2021, **6**, 1153.

8. X. Guo, S. Zheng, Y. Luo, H. Pang, *Chem. Eng. J.* 2020, **401**, 126005.

9. G. Li, Y. Tang, T. Fu, Y. Xiang, Z. Xiong, Y. Si, C. Guo, Z. Jiang, *Chem. Eng. J.* 2022, **429**, 132174.

10. L. Song, H. Fan, T. Wang, T. Xiang, M. Zhang, C. Hu, W. Zhou, J. He, *Energy Environ. Mater.* 2021, **43**, 365.

11. S. Ren, X. Duan, F. Ge, Z. Chen, Q. Yang, M. Zhang, H. Zheng, *Chem. Eng. J.* 2022, **427**, 131614.

12. L. Lin, H. Sun, X. Yuan, Y. Gu, Q. Mu, P. Qi, T. Yan, L. Zhang, Y. Peng, Z. Deng, *Chem. Eng. J.* 2022, **428**, 131225.

13. J. Li, Y. Kang, W. Wei, X. Li, Z. Lei, P. Liu, *Chem. Eng. J.* 2021, **407**, 127961.

14. H. Liu, J. Guan, S. Yang, Y. Yu, R. Shao, Z. Zhang, M. Dou, F. Wang, Q. Xu, *Adv. Mater.* 2020, **32**, 2003649.

15. X. F. Lu, S. L. Zhang, E. Shangguan, P. Zhang, S. Gao, X. W. D. Lou, *Adv. Sci. (Weinh)* 2020, **7**, 2001178.

16. Y. Lian, W. Yang, C. Zhang, H. Sun, Z. Deng, W. Xu, L. Song, Z. Ouyang, Z. Wang, J. Guo, Y. Peng, *Angew. Chem. Int. Ed. Engl.* 2020, **59**, 286.

17. D. Liu, B. Wang, H. Li, S. Huang, M. Liu, J. Wang, Q. Wang, J. Zhang, Y. Zhao, *Nano*

Energy 2019, **58**, 277.

18. H. Lei, S. Tan, L. Ma, Y. Liu, Y. Liang, M. S. Javed, Z. Wang, Z. Zhu, W. Mai, *ACS Appl. Mater. Interfaces* 2020, **12**, 44639.

19. Y. Niu, X. Teng, S. Gong, Z. Chen, *J. Mater. Chem. A* 2020, **8**, 13725.

20. X. Han, X. Ling, Y. Wang, T. Ma, C. Zhong, W. Hu, Y. Deng, *Angew. Chem. Int. Ed. Engl.* 2019, **58**, 5359.

21. X. Wu, S. Chen, Y. Feng, Q. Yuan, J. Gao, Y. Chen, Y. Huang, Y. B. He, W. Gan, *Mater. Today Phys.* 2019, **9**, 100132.

22. X. Hao, Z. Jiang, B. Zhang, X. Tian, C. Song, L. Wang, T. Maiyalagan, X. Hao, Z. J. Jiang, *Adv. Sci. (Weinh)* 2021, **8**, 2004572.

23. S. Li, X. Yang, S. Yang, Q. Gao, S. Zhang, X. Yu, Y. Fang, S. Yang, X. Cai, *J. Mater. Chem. A* 2020, **8**, 5601.

24. Y. Ma, D. Chen, W. Li, Y. Zheng, L. Wang, G. Shao, Q. Liu, W. Yang, *Energy Envir. Mater.* 2022, **5**, 543.

25. L. Liu, Y. Wang, F. Yan, C. Zhu, B. Geng, Y. Chen, S. l. Chou, *Small Methods* 2019, **4**, 2101116.